Chinese Chemical Letters 35 (2024) 109302

Contents lists available at ScienceDirect

Chinese Chemical Letters

journal homepage: www.elsevier.com/locate/cclet

Accurate expression of neck motion signal by piezoelectric sensor data analysis

Neng Shi[a,1], Haonan Jia[a,1], Jixiang Zhang[a], Pengyu Lu[a], Chenglong Cai[a], Yixin Zhang[a], Liqiang Zhang[a], Nongyue He[a], Weiran Zhu[b], Yan Cai[a,*], Zhangqi Feng[c], Ting Wang[a,*]

[a] State Key Laboratory of Digital Medical Engineering, National Demonstration Center for Experimental Biomedical Engineering Education, School of Biological Science and Medical Engineering, Southeast University, Nanjing 210096, China
[b] SceneRay Co., Ltd., Suzhou 215123, China
[c] School of Chemistry and Chemical Engineering, Nanjing University of Science and Technology, Nanjing 210094, China

ARTICLE INFO

Article history:
Received 23 September 2023
Revised 12 November 2023
Accepted 14 November 2023
Available online 17 November 2023

Keywords:
Piezoelectric transducer
Wavelet decomposition
Muscle motion signal
Signal analysis
Noise component
Healthcare monitoring

ABSTRACT

The development of high-precision sensors using flexible piezoelectric materials has the advantages of high sensitivity, high stability, good durability, and lightweight. The main problem with sensing equipment is low sensitivity, which is due to the mismatch between materials and analysis methods, resulting in the inability to effectively eliminate noise. To address this issue, we developed the denoising analysis method to motion signals captured by a flexible piezoelectric sensor fabricated from poly(L-lactic acid) (PLLA) and polydimethylsiloxane (PDMS) materials. Experimental results demonstrate that this improved denoising method effectively removes noise components from neck muscle motion signals, thus obtaining high-quality, low-noise motion signal waveforms. Wavelet decomposition and reconstruction is a signal processing technique that involves decomposing a signal into different scales and frequency components using wavelets and then selectively reconstructing the signal to emphasize specific features or eliminate noise. The study employed the sym8 wavelet basis for wavelet decomposition and reconstruction. In the denoised signals, a high degree of stability and periodic peaks are distinctly manifested, while amplitude and frequency differences among different types of movements also become noticeably visible. As a result of this study, we are enabled to accurately analyze subtle variations in neck muscle motion signals, such as nodding, shaking the head, neck lateral flexion, and neck circles. Through temporal and frequency domain analysis of denoised motion signals, differentiation among various motion states can be achieved. Overall, this improved analytical approach holds broad application prospects across various types of piezoelectric sensors, such as healthcare monitoring, sports biomechanics.

In recent years, flexible piezoelectric materials have been widely used in various fields, particularly in the development of flexible electronic and wearable devices [1]. However, there is still a lack of effective analytical methods that correspond to the motion signals captured by flexible sensors [2–4]. To address this gap, we have developed an innovative approach for analyzing motion signals, endowing transducer sensors with boundless potential and significance [5–7].

Piezoelectric sensors have garnered significant attention in research due to their high sensitivity, stable performance, durability, and lightweight properties [8,9]. Among the various sensor types available, piezoelectric sensors have emerged as a promising choice for wearable monitoring devices [10–12]. However, despite the presence of various sensor types in the market and corresponding signal processing and analysis methods, the accuracy of these methods is often questioned, making it difficult to determine which approach accurately matches different transducer materials [13,14]. It is particularly important to conduct in-depth research on signal processing and analysis methods to match the characteristics of flexible sensing materials for ensuring accurate results.

Common denoising methods for motion signals, such as Butterworth filtering, currently suffer from issues like signal blurring and loss of local features. Wavelet decomposition techniques play a crucial role in the detection and processing of motion signals [15,16]. They possess enhanced time-frequency analysis capabilities, facilitate multi-resolution analysis, effectively suppress noise, and aid in feature extraction, thereby providing reliable tools and methods for the analysis, recognition, and classification of motion

* Corresponding authors.
E-mail addresses: yancai@seu.edu.cn (Y. Cai), tingwang@seu.edu.cn (T. Wang).
[1] These authors contributed equally to this work.

https://doi.org/10.1016/j.cclet.2023.109302
1001-8417/

signals [17,18]. In the fields of healthcare, sports science and rehabilitation, wavelet decomposition holds extensive potential for applications. In this study, we conducted wavelet decomposition on motion signals using different wavelet bases. This approach preserves the characteristics of the original waveform while, by introducing denoising evaluation criteria, it identifies the optimal wavelet basis selection, specifically sym8, resulting in improved denoising efficacy.

In this study, flexible piezoelectric sensors were fabricated using original-fiber poly(L-lactic acid) (PLLA) material for monitoring neck muscle movements. The developed sensors exhibited high sensitivity and could detect subtle human motion signals. The sensors allowed real-time monitoring of neck muscle movements, and the data were captured using an electrochemical workstation. Moreover, these high-sensitivity sensors demonstrated excellent durability and stability. Additionally, we improved traditional physiological signal denoising methods by focusing on motion signals. In contrast to the limitations of conventional denoising approaches, we utilized wavelet analysis to enhance the denoising efficacy of motion signals, resulting in optimal low-noise motion signal waveforms. In our research, we further analyzed the variations in signals under different motion states and explored the variability between signals. As a result, we could better distinguish signals corresponding to different movements. The above results demonstrate that our proposed improved denoising method effectively removes high-frequency interference and low-frequency baseline drift, providing a more reliable foundation for subsequent muscle motion signal analysis. This novel approach to motion signal processing and analysis can better match transducer materials, thereby acquiring real-time accurate data.

The PLLA film was purchased from Aladdin Biochemical Technology Co., Ltd. The polydimethylsiloxane (PDMS) solution and the curing agent were obtained from the Dow Chemical Company. First, a mixture of curing agent and PDMS solution in a volume ratio of 1:10 was prepared and stirred using a magnetic rotor at room temperature for approximately 15–20 min until the microbubbles in the solution were dense and evenly distributed. Then, ultrasonic treatment was applied for 3–5 min to achieve complete bubble removal and produce the encapsulation material. PLLA films were cut into rectangular samples of 1.5 cm × 1.5 cm (one or two layers) as the conductive layer. Next, two rectangular aluminum foils of 1.8 cm × 1.5 cm were taken, and a 1 cm cut was made 0.3 cm away from the short side (1.5 cm), leaving a 0.5 cm × 0.3 cm connection as the signal path. These aluminum foils were used as the encapsulation layer. The PLLA film was attached to the 1.5 cm × 1.5 cm area of the aluminum foil, and the encapsulation material was preliminarily packaged around the PLLA film using a small-diameter syringe. Then, the second aluminum foil was added to complete the electrode fabrication. Finally, one side of the PLLA electrode was coated using a spin coater, and 0.1–0.15 mL of encapsulation material was dripped onto it (drop height of 3 cm, rotation speed of 3 k/min). The electrode was then placed in an oven at a constant temperature of 60 °C and dried for 12 h and cooled to room temperature before removal. The coating and drying process was repeated on the other side to achieve complete encapsulation. This procedure is illustrated in Fig. S1 (Supporting information).

The morphology of the samples was characterized using a scanning electron microscope (SEM). In addition, the samples were tested under different pressing conditions using a self-made pressure device to simulate practical use environments. Furthermore, the voltage and current changes of the samples under different pressures were measured using an electrochemical workstation to evaluate their piezoelectric properties. Before conducting the experiment to acquire neck movement signals, the sampling frequency of the electrochemical workstation software was set, and

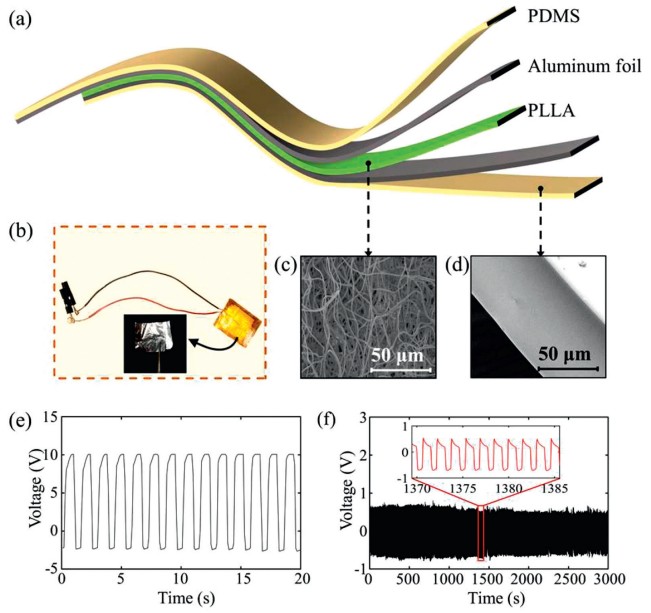

Fig. 1. (a) Schematic of a flexible piezoelectric sensor with a five-layer structure: PDMS encapsulation layer, aluminum foil for both conduction and additional encapsulation, and PLLA as the piezoelectric layer. (b) Photograph of PLLA electrode: The sensor electrode, being flexible and bendable, conforms easily to various shapes and surface curvatures. (c) Microscopic image of PLLA membrane under electron microscopy: a mesh-like structure formed from interwoven fibers. (d) PDMS membrane (longitudinal view): smooth surface with a relatively uniform diameter of approximately 30–40 μm. (e) Voltage of the high-sensitivity sensor. (f) Durability test of the high-sensitivity sensor for over 3000 s.

the participants were fully informed of the experimental procedures. The PLLA flexible piezoelectric sensor was affixed to the participant's left scapula and second thoracic vertebra using medical tape. The sensor, electrochemical workstation, and personal computer were connected, and the data acquisition software was opened for signal acquisition. After obtaining a sufficient number of neck movement signals, the collected data was saved for subsequent analysis.

In this study, traditional noise reduction methods, including Butterworth filtering, finite impulse response filtering, and Chebyshev filtering, were used to filter the neck movement signals. In addition, wavelet decomposition was used to process the movement signals to retain useful physiological signals and remove noise components. These methods effectively extracted physiological features from the neck movement signals, improved signal quality and reliability, and provided reliable data foundations for subsequent analysis and research.

The overall and local composition of the electrode is described in Fig. 1 shown as below. The flexible piezoelectric sensor composed of five layers of materials (Fig. 1a). PDMS functions as the encapsulation layer. The aluminum foil layer serves as both the conductive layer and another layer of encapsulation, enabling the conduction of charges within the sensor's interior and collaborating with the PDMS encapsulation layer to protect the internal structure and circuitry of the sensor. PLLA acts as the piezoelectric layer, enabling the capture and detection of motion signals. This multilayer structure provides excellent mechanical strength, stability, and effective encapsulation and protection. The fabricated sensor electrode is flexible and bendable characteristics, enabling it to conform to various shapes and surface curvatures (Fig. 1b). The details of PLLA fibers can be found in Fig. 1c, a mesh-like structure was formed from multiple fibers interwoven. This mesh structure offers high mechanical flexibility and sensitivity to voltage changes, enhancing the sensor's sensitivity and responsiveness to accurately perceive and convert pressure signals. Fig. 1d dis-

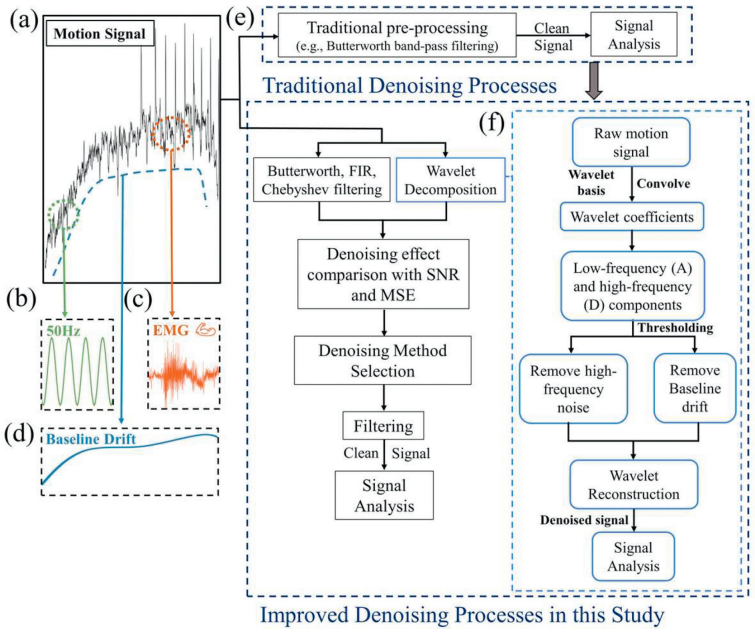

Fig. 2. (a) Neck muscle movement signals containing low-frequency and high-frequency interference. (b) Interference and noise in the form of 50 Hz mains interference caused by power line interference and high-order harmonic interference. (c) EMG interference noise caused by subjects' tension and subtle body movements during the data acquisition. (d) Baseline drift noise caused by human respiration and sensor temperature drift. (e) Traditional processes and the improved denoising processes: Introduce wavelet decomposition and reconstruction for denoising, and use SNR and RMSE indicators to evaluate the translation of denoising results. (f) Details of the wavelet decomposition and reconstruction denoising process.

plays an untreated PDMS membrane, exhibiting a smooth surface with a relatively uniform diameter of approximately 30–40 μm. The smooth surface helps reduce external interference and facilitates reliable signal transmission.

In order to further investigate the piezoelectric performance of the sensor, a certain level of force was applied to the sensor to test its sensitivity [19]. When the sensor was subjected to external force, the material's piezoelectric layer underwent internal polarization, resulting in positive and negative charges on both surfaces of the piezoelectric layer and generating an electric signal [20]. The voltage of the sensor was measured using an electrochemical workstation (Fig. 1e), which displayed the basic piezoelectric performance of the sensor. The output voltage and sensitivity analysis results of the sensor under various stress conditions can be seen in Fig. S2 (Supporting information). To obtain the piezoelectric performance of the piezoelectric sensor, a force was applied to the sensor at a frequency of 0.67 Hz, and the average output voltage of the sensor was found to be 10 V. In addition, the voltage amplitude only exhibited slight fluctuations under a fixed force of 0.67 Hz during 3000 s of fatigue testing (Fig. 1f), indicating the high stability and durability of the piezoelectric sensor. The voltage signals at the beginning, middle, and final stages of the sensor fatigue test all maintained good stability, as shown in Fig. S3 (Supporting information).

The main location for collecting neck movement motion signals is between the left scapula and the second thoracic vertebra. During the signal acquisition process, external noise signals can interfere and result in the presence of noise components in the collected neck movement signals (Fig. 2a). The main sources of noise in neck movement signals include power frequency interference, electromyographic (EMG) interference, baseline drift, and high-frequency noise from the human skin and external environment [21,22]. Power frequency interference mainly consists of 50 Hz power line interference and high-order harmonic interference, with low amplitude, appearing as regular small ripples on the waveform (Fig. 2b) [23]. Factors such as subject tension, subtle limb movements, and certain diseases during data acquisition can lead to the generation of EMG interference noise (Fig. 2c). The frequency spectrum of EMG interference is generally between 30 Hz and 300 Hz [24]. Among the various noise sources in neck muscle movement signals, baseline drift noise has the most significant impact on the signal. Baseline drift is mainly caused by human respiration and sensor temperature drift [25,26]. Compared with neck muscle movement signals, baseline drift is a low-frequency signal, ranging from 0.01 Hz to several hertz, with its main component around 0.1 Hz (Fig. 2d).

In the process of collecting neck movement signals, system noise and random noise inevitably interfere with the signals, causing baseline drift and high-frequency noise, which makes the analysis and processing of movement signals inconvenient [27]. Therefore, it is of great significance to study effective methods for removing these noises from physiological signals. Traditionally, various signal pre-processing techniques, such as Butterworth filter, finite impulse response (FIR) filter, and Chebyshev filter, are commonly employed to mitigate noise in physiological signals [28]. However, despite the use of these filtering methods, eliminating noise remains challenging, significantly impacting the accuracy of subsequent analyses.

To address this issue, this study proposes an improved filtering method based on the characteristic features of muscle movement signals to remove interference. This method introduces wavelet decomposition and reconstruction into the conventional denoising process and evaluates the results using signal-to-noise ratio (SNR) and root mean squared error (RMSE) as comparison metrics for different denoising methods [29]. This step is crucial for effective denoising of muscle movement signals. Fig. 2e depicts a schematic representation of the conventional approach and the novel method proposed in this study. By contrasting the enhanced denoising process with the traditional procedure, the diagram visually presents the concrete process of motion signal processing.

Common physiological signal denoising methods include Butterworth filtering, FIR filtering, and Chebyshev filtering [30]. This

study incorporates wavelet decomposition and re-construction in addition to commonly used denoising methods. Wavelet decomposition and reconstruction are employed to decompose the motion signals, eliminating low-frequency baseline drift and high-frequency noise, and subsequently reconstructing the denoised signal from the valuable components. The specific process is illustrated in Fig. 2f. In the following, the principles of these methods will be introduced, and their denoising effects will be compared to select the optimal method.

The Butterworth filter has a relatively flat passband, and as the filter order increases, the transition band becomes steeper, and the stopband suppression increases [31]. Since the main frequency range of neck muscle movement signals is around 0.3 Hz and the baseline drift signals are distributed around 0.1 Hz, we use a minimum order Butterworth filter for 0.1 Hz high pass filtering of the movement signals. The processed waveform is shown in Fig. S4a (Supporting information). The FIR filter is a common digital filter with a finite-length unit impulse response. The FIR filter can obtain a strict linear phase characteristic while satisfying the amplitude-frequency response requirements [32]. We use an FIR filter to process the neck movement signals, and the processed waveform is shown in Fig. S4b (Supporting information). The Chebyshev filter has a faster transition band attenuation rate than the Butterworth filter, but its frequency response within the passband is not as flat as the latter. The Chebyshev filter is divided into two types: Type I and Type II [33]. In Type I Chebyshev filter, the ripple amplitude inside the passband is equal, while in Type II, the ripple amplitude inside the stopband is equal [34]. We use a second-order Type I Chebyshev filter to process the noisy movement signals, and the processed waveform is shown in Fig. S4c (Supporting information).

Wavelet analysis is a signal analysis tool based on local features, which decomposes the signal into wavelet coefficients of different frequency bands, revealing the signal's time-frequency characteristics [35,36]. Applying wavelet de-composition to denoise motion signals involves decomposing the signal into frequency components, and then filtering the decomposition coefficients based on the characteristics of wavelet decomposition to remove noise components and preserve the physiological signal's characteristic components, ultimately reconstructing the denoised motion signal [37]. Compared to traditional filtering methods, wavelet decomposition is better suited for handling non-stationary signals and allows for the selection of suitable wavelet bases for decomposition, offering greater flexibility and adaptability [38]. In this study, the symmetrical wavelet basis (sym wavelet) was used for wavelet decomposition of motion signals, removing baseline drift and high-frequency noise signals in the 0–0.4 Hz range, resulting in the denoised waveform shown in Fig. S4d (Supporting information).

Compared with traditional denoising methods such as Butterworth and Chebyshev filters, which can effectively reduce noise, there may be blurring and loss of local features of the signal. The FIR filtering method has drawbacks such as time-domain waveform distortion and phase distortion, resulting in unsatisfactory denoising effects [39]. The wavelet transform denoising method can filter out noise components in the signal while retaining the original waveform characteristics. To evaluate the effectiveness of the traditional denoising methods and the wavelet decomposition denoising method, we introduced two evaluation metrics: SNR and RMSE. SNR describes the ratio between the effective components and noise components in the signal, measured in dB, and can be calculated using Eq. 1. A higher SNR value indicates better denoising performance of the method.

$$\mathrm{SNR} = 10\log\frac{\sum_{i=1}^{N} f^2(i)}{\sum_{i=1}^{N}\left(g(i)-f(i)\right)^2} \tag{1}$$

Table 1
Denoising results of noisy motion signal.

Method	Signal power (W)	Noise power (W)	SNR (dB)	RMSE (V)
Butterworth	118.1979	5.6292	13.2216	0.0808
FIR	132.0387	6.9892	12.7627	0.0900
Chebyshev	95.2499	4.9578	12.8358	0.0758
sym7	95.7672	1.5602	17.8803	0.0425
sym8	99.0651	1.1764	19.2538	0.0369
db6	90.2074	2.3401	15.8601	0.0521
db7	90.1698	2.3663	15.8098	0.0524
coif3	94.6351	1.7077	17.4365	0.0445
coif5	95.7817	1.5611	17.8786	0.0426

where $f(i)$ denotes the original motion signal before denoising, $g(i)$ represents the motion signal after denoising, N stands for the length of the signal, and $i = 1, 2, 3, \ldots, N$.

The RMSE describes the closeness between the denoised signal and the original signal, as shown in Eq. 2. A smaller RMSE value indicates a closer match between the denoised signal and the original signal, thereby better preserving the useful information in the original signal.

$$\mathrm{RMSE} = \sqrt{\frac{1}{N}\sum_{i}^{N}\left(f(i)-g(i)\right)^2} \tag{2}$$

Using six different wavelet bases and combining three traditional denoising methods, the denoising results for the same motion signal are presented in Table 1. It can be observed that wavelet decomposition exhibits superior denoising performance. Specifically, the sym8 wavelet basis yields the highest SNR and the smallest RMSE after denoising the noisy motion signal, indicating the best denoising effectiveness.

In conclusion, compared to traditional filtering methods, wavelet decomposition denoising exhibits superior flexibility and adaptability, providing denoised results with higher SNR and lower RMSE. By selecting appropriate wavelet bases for decomposition according to specific requirements, it can effectively handle non-stationary signals. Consequently, wavelet decomposition denoising emerges as an excellent signal denoising technique.

Baseline drift noise is a low-frequency noise that has frequencies lower than the primary frequencies of human muscle movement waveforms. In order to extract the baseline drift from the original signal, an 8-level decomposition of the motion signal using the sym8 wavelet basis is performed, as shown in Fig. 3a. The frequency range corresponding to the approximate component of a_8 is approximately 0–0.1 Hz, which represents the baseline drift, as shown in Fig. 3b. Meanwhile, the d_1 and d_2 components represent high-frequency interference in the motion signal. By completely removing these high-frequency interferences and the baseline drift signal, and then reconstructing the remaining signal using wavelet reconstruction on the other levels, a denoised signal can be obtained.

As shown in Fig. 3c, the motion signal waveform contains baseline drift and high-frequency noise. The denoising result is shown in Fig. 3d. In the 0–90 s period, the neck motion is nodding, and the signal is relatively stable, with periodic peaks and similar peak values. According to the processed signal, at 90 s, the motion changes to shaking, and the signal fluctuates greatly with decreased peak values. The signal then remains stable until around 160 s, after which the motion changes to neck lateral flexion, with periodic peaks and similar peak heights lasting for about 2 min. Around 280 s, the movement changes to neck circles with increased amplitude and periodicity.

When people work for a long time without exercising, the muscles in their neck can become strained, leading to cervical spondylosis over time. Therefore, in order to reduce the incidence of

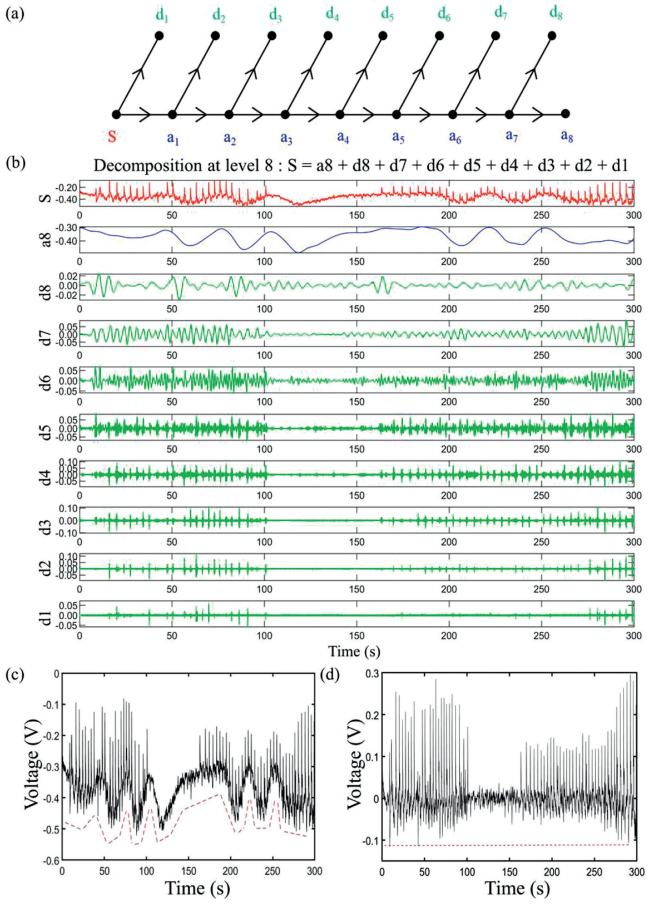

Fig. 3. (a) Wavelet decomposition tree: S represents the original signal, which is decomposed into low-frequency components (a_1–a_8) and high-frequency components (d_1–d_8) based on their frequency differences. (b) Eight-level wavelet decomposition of the motion signal: The signal is decomposed into a low-frequency component a_8 and high-frequency components (d_1–d_8). Notably, where a_8 exhibits a similar drift trend to the original signal. (c) Raw signal with baseline drift and high-frequency noise. (d) Signal after wavelet decomposition denoising: The removal of baseline drift and high-frequency interference results in a clear signal, significantly enhancing the distinguishability between different movements.

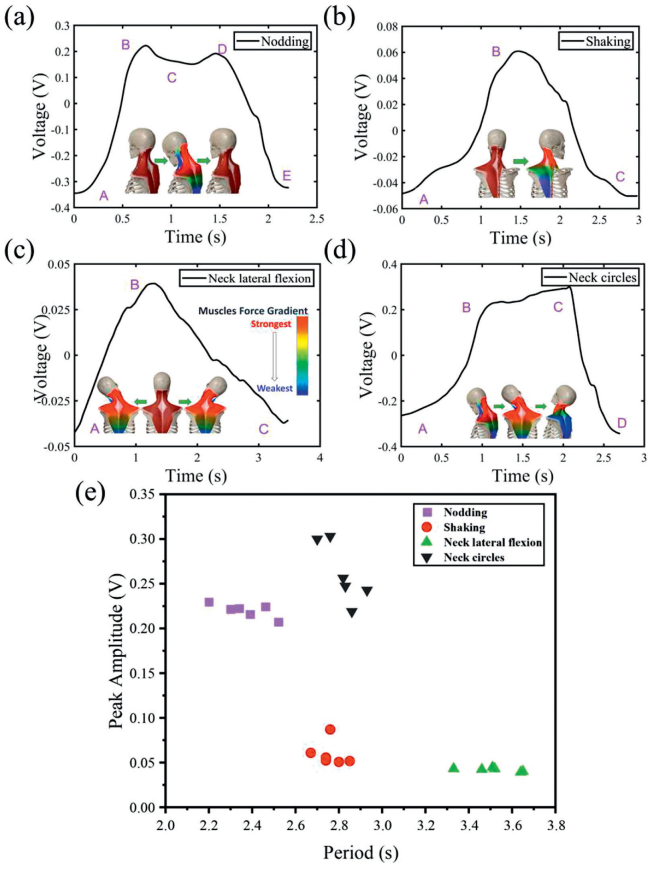

Fig. 4. Differentiated analysis of piezoelectric signals for various motions and scatter plot of neck muscle movement signals. (a) Nodding motion: two voltage peaks occur with amplitudes of approximately 0.22 V and a motion cycle of approximately 2.3 s. (b) Shaking: the piezoelectric sensor exhibits voltage peaks of approximately 0.06 V with a period of 2.7 s. (c) Neck lateral flexion: the piezoelectric sensor registers a peak voltage of approximately 0.04 V with a duration of 3.5 s. (d) Neck circles: a peak voltage of around 0.26 V is observed, with a period lasting 2.8 s. (e) Scatter plot of neck muscle movements periods and amplitudes, the *x*-axis represents the period (s), and the *y*-axis represents the peak value (V), significant variations in both period and amplitude among different motions.

cervical spondylosis, we use high-sensitivity sensors to monitor the movements of the subject's neck. During the test, a high-sensitivity sensor with medical adhesive tape was fixed to the area between the subject's left scapula and the second thoracic vertebra, as shown in Fig. S5a (Supporting information), to primarily perform four movements (nodding, shaking, neck lateral flexion and neck circles) to monitor the motion signals of the subject's neck muscles. When the subject performs the above-mentioned movement test, different movements will cause different stretching states of the neck muscles, and the different states will lead to changes in the force on the sensor, thereby forming different piezoelectric signals. The remain figures show the waveforms corresponding to the four movements of the subject, and the amplitudes and periods of different movements vary (Figs. S5b–e in Supporting information).

When the subject performs neck muscle movement, the periodicity of the action is maintained, so the piezoelectric signal is also periodic. Next, the signals of one cycle of different actions are analyzed to determine the corresponding relationship between the action and the amplitude.

Fig. 4a displays the piezoelectric signals generated by neck muscle movements during a nodding motion, with A to E denoting the process of completing one nod. During this process, the nodding motion exerts a force on the sensor, thereby generating a certain voltage signal. From A to B, the participant slowly lowers their head, during which the fiber bundles of the left trapezius muscle are stretched, and the left sternocleidomastoid muscle is in a contracted state, leading to an increase in the piezoelectric signal. At point B, the head reaches its lowest point, at which the left trapezius muscle is stretched to its maximum [40], and the sensor is subjected to the maximum force, resulting in the highest voltage signal. From B to C, the participant raises their head, and the sternocleidomastoid muscle is stretched [41], while the fiber bundles of the left trapezius are in a relaxed state, leading to a decrease in the sensor signal, indicating the recovery of muscle tension, resulting in a lower signal at point C. From C to D, the voltage amplitude fluctuates and reaches its peak again, due to the instant mechanical force generated by the contraction of the left trapezius as the head returns to its normal position, which triggers a response in the pressure sensor, thereby causing the fluctuation in the voltage amplitude. From D to E, the neck muscles are in a relaxed state, and there is no instantaneous mechanical force generated, so the sensor cannot sense any external force, and the voltage drops to its initial value. During the nodding motion, the voltage peak is approximately 0.22 V, and the motion cycle is 2.3 s.

The signal of neck muscle movement during the subject's head shaking action is shown in Fig. 4b, and the complete shaking process from A to C is illustrated. From A to B, the subject rotates their head horizontally to the left. At this time, the left

sternocleidomastoid and the fiber bundle of the left trapezius muscle are stretched, and the right splenius capitis contracts, resulting in an increase in force on the sensor and an increase in the piezoelectric signal. At point B, the head reaches the left extreme point, and the force on the sensor reaches the maximum value, resulting in the maximum amplitude of the piezoelectric signal. From B to C, the subject's head returns from left to right, and the force on the sensor decreases rapidly, leading to a rapid decrease in amplitude and completing the shaking action. During this process, the fibers of the left trapezius muscle continue to relax, while the right splenius capitis receives increased force. As the piezoelectric sensor is attached between the left scapula and the second thoracic vertebra, the main muscle force acting on the sensor during the B to C process is the right splenius capitis, and the force on the sensor decreases continuously, returning to the initial value. When the subject performs the head shaking action, the peak value of the piezoelectric sensor is about 0.06 V, and the period is 2.7 s.

As shown in Fig. 4c, this displays the output signal of neck muscle movement during the subject's neck lateral flexion motion. The process from A to C represents the completion of a head turning motion. During this process, the head turning motion will exert pressure on the sensor, generating a certain piezoelectric signal. During the process from A to B, the subject turns their head towards the left shoulder, causing the left sternocleidomastoid muscle to contract, stretching the left trapezius muscle, increasing the force on the neck muscles, and rapidly increasing the piezoelectric signal of the sensor. At point B, the head reaches the left extreme point, and the force on the sensor reaches the maximum value, with the voltage amplitude reaching its peak. From B to C, the subject's head turns towards the right shoulder, during which the left trapezius muscle is in a relaxed state, the left sternocleidomastoid muscle continues to stretch, and the right trapezius muscle is stretched. The force on the sensor, attached to the left scapula, decreases rapidly, and the voltage amplitude drops quickly to its initial value. During this motion, the peak voltage of the piezoelectric sensor is approximately 0.04 V, with a period of 3.5 s.

The output signal of neck muscle movement during the neck circles action of the subject is shown in Fig. 4d, and A to D represent the process of completing a head rotation action. During the A to B phase, the participant bends their head downwards in a motion similar to nodding, causing the fibers of the left sternocleidomastoid muscle to stretch and the muscle to relax, resulting in a slow increase in the piezoelectric signal. At point B, the head is at its lowest point. From B to C, the head rotates to the left rear in a circular motion, causing further stretching of the fibers of the left trapezius muscle, and resulting in a continuous increase in force on the piezoelectric sensor. At point C, the head and neck complete the extension motion, with the fibers of the left trapezius muscle at their maximum tension, causing the sensor force to peak and the maximum voltage signal to appear at point C. From C to D, the head completes the remaining circular motion from back to front right, with the left trapezius muscle relaxing and the left sternocleidomastoid muscle fibers in a stretched state. The piezoelectric sensor signal gradually drops to its initial value. During the neck circles motion, the peak sensor voltage is approximately 0.26 V, and the period is 2.8 s.

The scatter plot in Fig. 4e shows the relationship between voltage amplitude and period for different neck muscle movements. The purpose of this scatter plot is to compare the characteristics and differences of four distinct actions. The data for the scatter plot comes from measured neck muscle movement data, where the *x*-axis represents the period (s), and the *y*-axis represents the peak value (V). Each data point represents one specific movement, with its position determined by the period and amplitude. Upon observation, we find that the data points for the different movements exhibit distinct separation and clustering effects on the scatter plot. This indicates significant variations in both period and amplitude among the four actions. Specifically, the data points for nodding and neck lateral flexion movements are widely dispersed along the *x*-axis, indicating larger variations in the periods of these two movements. In contrast, the peak voltage values for these movements remain relatively stable at different times. On the other hand, the data points for shaking and neck circles movements are widely dispersed along the *y*-axis, indicating greater variations in peak voltage values for these two actions. In comparison, the periods of these movements show relatively smaller variations. In conclusion, the results from the scatter plot further validate the effectiveness of using period and amplitude to distinguish between different movements. Nodding and neck lateral flexion movements exhibit larger variations in period, while shaking and neck circles movements exhibit larger variations in peak voltage. These findings provide strong support for a deeper understanding of movement characteristics and mechanisms.

In conjunction with PLLA sensor for muscle movement recognition, the work has tailored a set of data analysis methods to accurately quantify and effectively identify neck motion information. Traditional motion signal processing algorithms were improved by incorporating wavelet decomposition for motion signal processing. The optimal denoising approach was determined by combining signal-to-noise ratio and mean squared error evaluations. This resulted in a signal analysis method that is compatible with the new type of sensor. Additionally, this analysis method proves effective for various types of piezoelectric sensors currently available.

We improved the signal processing procedure to mate the algorithms with our sensor in monitoring neck muscle movements in real-time. Through comparative denoising methods, we ultimately adopted wavelet decomposition for signal processing, effectively eliminating baseline drift and high-frequency noise. Analyzing the denoised motion signals, we studied the specific force exerted on neck muscles, and the results indicated that the signals corresponded accurately to specific movements, enabling precise identification of various neck actions. Finally, analyzing the scatter plot of motion signals revealed that the period and voltage amplitude could serve as distinguishing features for action recognition.

In conclusion, the transducer material-based high-sensitivity flexible piezoelectric sensor provides a reliable solution for monitoring neck muscle movements with superior performance in capturing subtle motion signals. This research has significant implications in physiological movement analysis and offers valuable reference for wearable monitoring device development. Finally, although the experimental outcomes of this study demonstrate the effectiveness of the improved signal processing and analysis approach, we still require a larger sample size of signals to train our computational method for improved universality and accuracy.

Declaration of competing interest

The authors declare that they have no known competing financial interests or personal relationships that could have appeared to influence the work reported in this paper.

Acknowledgments

The authors acknowledge the National Key R&D Plan (No. 2017YFA0205304) and NSFC (Nos. 61821002, 12072074). Thanks to SceneRay Co., Ltd. and Nanjing Chipsemi Electronic Technology Co., Ltd. for the financial support.

Supplementary materials

Supplementary material associated with this article can be found, in the online version, at doi:10.1016/j.cclet.2023.109302.

References

[1] G. Li, D. Wen, Chin. Chem. Lett. 32 (2021) 221–228.
[2] H. Zhao, M. Shu, Z. Ai, et al., Adv. Energy Mater. 12 (2022) 2201132.
[3] J. Liu, E. Chen, Y. Wu, et al., Adv. Compos. Hybrid Mater. 5 (2022) 1196–1205.
[4] W. Babatain, U. Buttner, N.E. Atab, M.M. Hussain, ACS Nano 16 (2022) 20305–20317.
[5] Y. Xie, Z. Li, Chem 4 (2018) 943–971.
[6] Y. Qin, J. Li, X. Zhang, et al., Chin. Chem. Lett. 34 (2023) 108826.
[7] Y. Chen, Z. Gao, F. Zhang, Z. When, X. Sun, Exploration 2 (2022) 20210112.
[8] M. Pohanka, Int. J. Electrochem. Sci. 12 (2017) 496–506.
[9] L. Xie, Z. Zhang, Q. Wu, et al., Chem. Sci. 15 (2023) 405–433.
[10] U. Proske, A.K. Wise, J.E. Gregory, Prog. Neurobiol. 60 (2000) 85–96.
[11] G. Li, J. Li, Z. Li, et al., Adv. Compos. Hybrid Mater. 5 (2022) 766–775.
[12] X. Wang, Y. Huan, S. Ji, et al., Nano Energy 101 (2022) 107580.
[13] E. Capuana, F. Lopresti, M. Ceraulo, V.L. Carrubb, Polymers 14 (2022) 1153 (Basel).
[14] F. Sadraei, M. Ghollasi, F. Khakpai, R. Halabian, H.J. Tehrani, Regen. Ther. 21 (2022) 263–270.
[15] S. Shahtalebi, S.F. Atashzar, R. Patel, A. Mohammadi, Biomed Signal Process. 48 (2019) 179–188.
[16] T. Tuncer, S. Dogan, A. Subasi, Biomed. Signal Process. 58 (2020) 101872.
[17] M. Grobbelaar, S. Phadikar, E. Ghaderpour, et al., Signals 3 (2022) 577–586.
[18] S. Qaisar, S. Khan, D. Dallet, R. Tadeusiewicz, P. Pławiak, Biocybern. Biomed. Eng. 42 (2022) 681–694.
[19] S. Qian, L. Qin, J. He, et al., Mater. Lett. 261 (2020) 127119.
[20] N.R. Alluri, S. Selvarajan, A. Chandrasekhar, et al., Compos. Sci. Technol. 142 (2017) 65–78.
[21] S. Liu, X. Meng, J. Zhang, J. Chae, Biosens. Bioelectron. 139 (2019) 111336.
[22] A. Kensert, G. Collaerts, K. Efthymiadis, et al., J. Chromatogr. A 1646 (2021) 462093.
[23] R.B. Vidhya, S. Jerritta, Mater. Today Proc. 49 (2022) 2955–2961.
[24] H. Li, X. Wang, L. Chen, E. Li, Circ. Syst. Signal Process. 33 (2014) 1261–1276.
[25] R. Sharma, R. Pachori, Biomed. Signal Process. 45 (2018) 33–49.
[26] A. Singhal, P. Singh, B. Fatimah, R.B. Pachori, Biomed. Signal Process. 57 (2020) 101741.
[27] Z. Izakian, M.S. Mesgari, R. Weibel, Eng. Appl. Artif. Intell. 88 (2020) 103394.
[28] J. Kim, K. Lee, J. Lee, K. Kim, J. Supercomput. 74 (2018) 6785–6793.
[29] K. Todros, R. Winik, J. Tabrikian, Signal Process. 108 (2015) 622–627.
[30] W. Laghari, M. Baloch, M. Mengal, S. Shah, Circ. Syst. 5 (2014) 209–216.
[31] M. Liu, H.Q. Hao, P. Xiong, et al., J. Med. Biol. Eng. 38 (2018) 980–992.
[32] A. Kumar, H. Tomar, V. Mehla, R. Komaragiri, M. Kumar, ISA Trans. 114 (2021) 251–262.
[33] J.D. Rhodes, S.A. Alseyab, Int. J. Circ. Theor. Appl. 8 (1980) 113–125.
[34] S.S. Bhogeshwar, M.K. Soni, D. Bansal, Int. J. Biomed. Eng. Technol. 16 (2014) 244–267.
[35] B. Xie, Z. Xiong, Z. Wang, et al., Nucl. Eng. Technol. 52 (2020) 1771–1776.
[36] S. Chatterjee, R.S. Thakur, R.N. Yadav, L. Gupta, Signal Process. 198 (2022) 108605.
[37] B. Yu, EURASIP J. Image Video Process. 2019 (2019) 5.
[38] C. Kaur, A. Bisht, P. Singh, G. Joshi, Biomed. Signal Process. 65 (2021) 102337.
[39] S. Kar, M. Ganguly, Mater. Today Proc. 58 (2022) 437–444.
[40] D.G. Simons, S. Mense, Pain 75 (1998) 1–17.
[41] D. Falla, A. Rainoldi, R. Merletti, G. Jull, Clin. Neurophysiol. 114 (2003) 488–495.